Available online at www.sciencedirect.com
ScienceDirect
Mathematics and Computers in Simulation 72 (2006) 242–248
MATHEMATICS AND COMPUTERS IN SIMULATION
www.elsevier.com/locate/matcom

Modeling fluid flow in fuel cells using the lattice-Boltzmann approach

Lian-Ping Wang*, Behnam Afsharpoya

Department of Mechanical Engineering, University of Delaware, Newark, DE 19716-3140, USA

Available online 14 July 2006

Abstract

Two flow problems relevant to fuel cell modeling are simulated with the lattice-Boltzmann (LB) approach. The first is a 3D viscous flow through a section of serpentine channel and the second is a 2D channel filled or partially filled with porous medium. In the first case, attention is given to the implementation details such as inlet–outlet boundary conditions, nonuniform grid, and forcing. It was shown that the flow pattern and pressure distribution depends sensitively on the flow Reynolds number as the flow Reynolds number is increased from 10 to 1000. There also appears to be some evidence that the transition to a turbulent flow occurs at Reynolds number on the order of 1000. In the second case, the effects of multiple time scales and interface between the porous medium and clear channel are considered. It was shown that, in order to obtain correct results at the interface or near the boundary, the physical time scales of the problem must be kept larger than the lattice time. This can be achieved by using a small particle velocity in the LB scheme.

Keywords: Lattice Boltzmann approach; Fuel cells; Serpentine channel; Porous medium; Pressure loss

1. Introduction

Fuel cells are electrochemical reactors generating electricity directly from oxidation reactions of fuels. Due to their high efficiency (typically twice of the energy conversion efficiency of internal combustion engines), near-zero emissions, low noise, and portability, fuel cells are being considered as a potentially viable energy-conversion device for mobile, stationary, and portable power. The low operation temperature of the proton-exchange membrane fuel-cell (PEMFC) makes it a preferred fuel-cell type for automotive applications. A PEMFC unit consists of two thin, porous electrodes (an anode and a cathode) separated by a membrane-electrode assembly. Reactants (e.g., hydrogen and air) are brought into the cell through flow distribution channels (Fig. 1a). Computational models of increasing complexity are currently being developed to better understand issues related to the performance of PEMFC, such as pressure loss and temperature distribution in the flow channels, species transport through porous gas diffusion layers, and water management on the cathode side. Wang [11] provides a review of recent modeling efforts using traditional computational fluid dynamics (CFD) based on macroscopic conservation equations.

* Corresponding author.
E-mail address: lwang@udel.edu (L.-P. Wang).

0378-4754/$32.00 © 2006 IMACS. Published by Elsevier B.V. All rights reserved.
doi:10.1016/j.matcom.2006.05.038

Here we explore the use of lattice-Boltzmann (LB) approach as a modeling tool for predicting fluid flows relevant to PEMFC. The LB approach is based on a kinetic formulation and could have certain advantages over the traditional CFD [1,9]. While LB models capable of addressing thermal flows, flows through porous media, multiphase flows, electro-osmotic flows, and contact line, etc., have been proposed in recent years, two general aspects remain to be studied before they can be applied to fuel-cell modeling. The first aspect concerns the accuracy and reliability of these models for practical applications. Since these models have typically only been tested for idealized problems, their applications to PEMFC flow problems need to be critically examined and different possible LB models be compared. The second aspect concerns a variety of implementation issues when dealing with practical applications, such as nonuniform grid, forcing implementation, boundary conditions, and porous-medium interface.

In this paper, we consider these aspects using two flow problems related to PEMFC. The first is viscous flow through a section of serpentine flow channel (Fig. 1b) and we explore how to optimally and efficiently implement an LB approach. The second problem is flow through porous media for which multiple time and length scales exist.

2. Flow through a section of serpentine channel

Here we investigate the pressure distribution and flow pattern in a section of serpentine channel (Fig. 1a) over a range of Reynolds numbers encountered in PEMFC. The channel has a square cross section of width W and a side length L (Fig. 1b). As a first step, we consider isothermal laminar flow and neglect the flow into the gas diffusion layer so that the back wall is treated as a no-slip wall. This similar flow was studied recently by Maharudrayya et al. [7] using a traditional finite-volume CFD code.

The LB equation for the distribution function (DF) f_i of the particle with velocity $\mathbf{e}_i$:

$$f_i(\mathbf{x}+\mathbf{e}_i\delta_t, t+\delta_t) - f_i(\mathbf{x},t) = -\tfrac{1}{\tau}[f_i(\mathbf{x},t) - f_i^{(\mathrm{eq})}(\mathbf{x},t)] + \psi_i(\mathbf{x},t) \tag{1}$$

is solved with a prescribed forcing field ψ_i designed to model the pressure difference between the inlet and the outlet, so that a periodic boundary condition can still be applied to f_i between the inlet and outlet. This minimizes the density fluctuations associated with f_i which could otherwise be significant considering the large L/W ratio here and the augmented pressure loss through the bend. The D3Q19 model [9] is used with the following equilibrium distribution function:

$$f_i^{(\mathrm{eq})}(\mathbf{x},t) = \omega_i\rho\left[1 + \frac{\mathbf{e}_i\cdot\mathbf{u}}{c_\mathrm{s}^2} + \frac{\mathbf{uu}:(\mathbf{e}_i\mathbf{e}_i - c_\mathrm{s}^2\mathbf{I})}{2c_\mathrm{s}^4}\right], \tag{2}$$

where ω_i is the weight, the sound speed c_s is $1/\sqrt{3}$, and $\mathbf{I}\equiv[\delta_{ij}]$ is the second-order identity tensor.

Two different methods of specifying the forcing term were tested. The first method specifies ψ_i and macroscopic variables as

$$\psi_i(\mathbf{x},t) = \omega_i\mathbf{e}_i\cdot\mathbf{F}/c_\mathrm{s}^2, \qquad \rho = \sum_i f_i, \qquad \rho\mathbf{u} = \sum_i f_i\mathbf{e}_i, \qquad p = \rho c_\mathrm{s}^2 + p_0(\mathbf{x}), \tag{3}$$

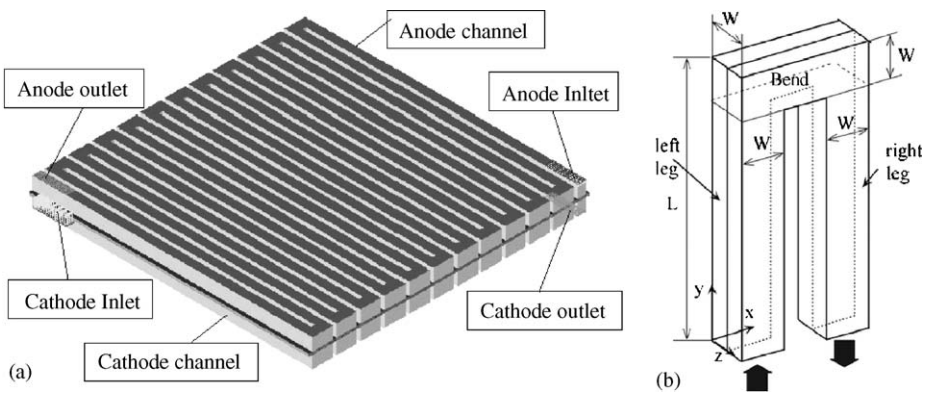

Fig. 1. (a) Sketch of serpentine flow channel in PEM fuel cell. (b) A section of the channel being modeled.

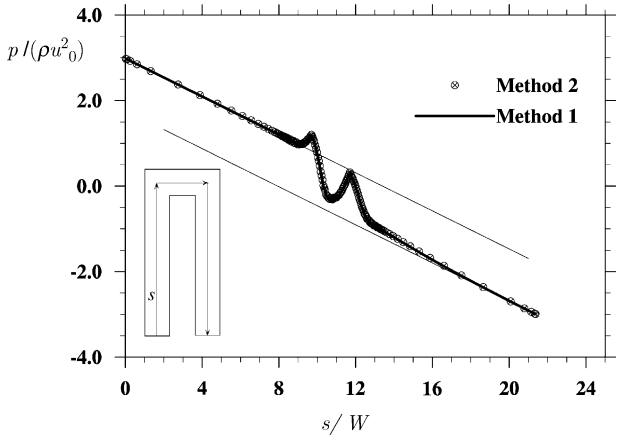

Fig. 2. The pressure as a function of the distance s along the centerline of the channel when $Re = 127$.

where ρ, $\mathbf{u}$, and p are the fluid density, velocity, and pressure, respectively. The macroscopic force field is defined as $\mathbf{F} = (0, A(1 - y/L_1), 0)$ for the left leg of the channel and $\mathbf{F} = (0, -A(1 - y/L_1), 0)$ for the right leg, with $L_1 = L - W$. In the bend region, $\mathbf{F} = 0$. This force field amounts to an auxiliary pressure field of $p_0(\mathbf{x}) = A(L_1 - y)^2/(2L_1)$ in the left leg and $p_0(\mathbf{x}) = -A(L_1 - y)^2/(2L_1)$ in the right leg and a total pressure difference of AL_1 between the inlet and outlet (the driving force for the flow). The coefficient A was set to $8\rho\nu v_0/W^2$, where the kinematic viscosity is related to the relaxation time as $\nu \equiv (\tau - 0.5)c_s^2\delta_t$ and v_0 is a velocity scale (of similar magnitude as the mean flow speed u_0). Guo et al. [3] showed that the forcing term in the above formulation introduces some lattice effects to the Navier–Stokes equation. They were able to remove the lattice effects by modifying the definition of ψ_i and $\mathbf{u}$ as

$$\psi_i(\mathbf{x}, t) = \omega_i \left(1 - \frac{1}{2\tau}\right) \left[\frac{\mathbf{e}_i \cdot \mathbf{F}}{c_s^2} + \frac{\mathbf{uF} : (\mathbf{e}_i\mathbf{e}_i - c_s^2\mathbf{I})}{c_s^4}\right], \qquad \rho\mathbf{u} = \sum_i f_i\mathbf{e}_i + \frac{\delta_t}{2}\mathbf{F}. \tag{4}$$

This improved method is referred to as the second method. We found that the two methods gave almost identical results, namely the thick solid line and the symbols overlap almost exactly in Fig. 2.

A nonuniform mesh along the y-direction (see Fig. 1b) is necessary for this 3D channel flow for computational efficiency. We have developed a Lagrangian interpolation method to compute DF at a grid point (the point marked with a small circle in Fig. 3) from the DFs on shifted grid points (points marked by small squares in Fig. 3) surrounding the grid point. Note that the Lagrangian interpolation utilizes three lattice nodes in each direction. In any direction for which the grid is uniform, it recovers exactly the usual streaming step in the LB scheme. The method generalizes the interpolation-supplemented LB method of He et al. [6] and is easier to implement than the Taylor series expansion and least squares-based LB method of Shu et al. [10]. Depending on the flow Reynolds number Re, the number of nonuniform grid points varies from 63 to 123 along the y-direction with L/W used ranging from 10 to 22. The cross section of the channel is mapped by a uniform lattice with the number of lattice points over the width W ranging from 21 to 41. The walls are located in the middle of lattice links so a second-oder accuracy is achieved with a simple bounce-back implementation.

Fig. 2 shows a typical pressure distribution along the centerline of the channel. If the channel is made very long ($L \gg W$), the pressure should change linearly with distance away from the bend region at both the inlet and outlet, with a same slope. This slope away from the bend, indicated by the two thin straight lines in Fig. 2, can be used to define a friction factor for a straight channel (i.e., $f = W\Delta p/(L\rho u_0^2/2)$) and the results are shown in Fig. 4a as a function of flow Reynolds number Re. This friction factor can be well modeled by the friction factor in a circular pipe (i.e., $f = 64/Re$) with diameter defined as $D = 2W/\sqrt{\pi}$, namely, diameter corresponding to same cross-sectional area. The deviation at large Re could be due to the influence of the bend since the value of L used ($L = 22W$) is not long enough.

A finite jump in pressure due to the bend exists, as indicated by the vertical distance between the two thin parallel lines in Fig. 2. This is referred to as the bend pressure loss. The ratio of this jump to the slope away from the bend region defines a normalized, equivalent length for the bend pressure loss, $\Delta L_B/W$. This equivalent length is shown in Fig. 4b as a function of Re. Of importance is that this length increases quickly with Re to values comparable to the

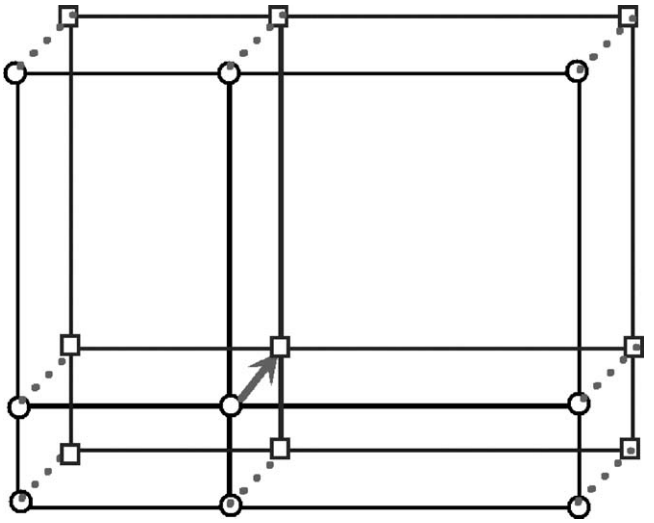

Fig. 3. Sketch showing the grid locations (circles) and the shifted grid locations (squares).

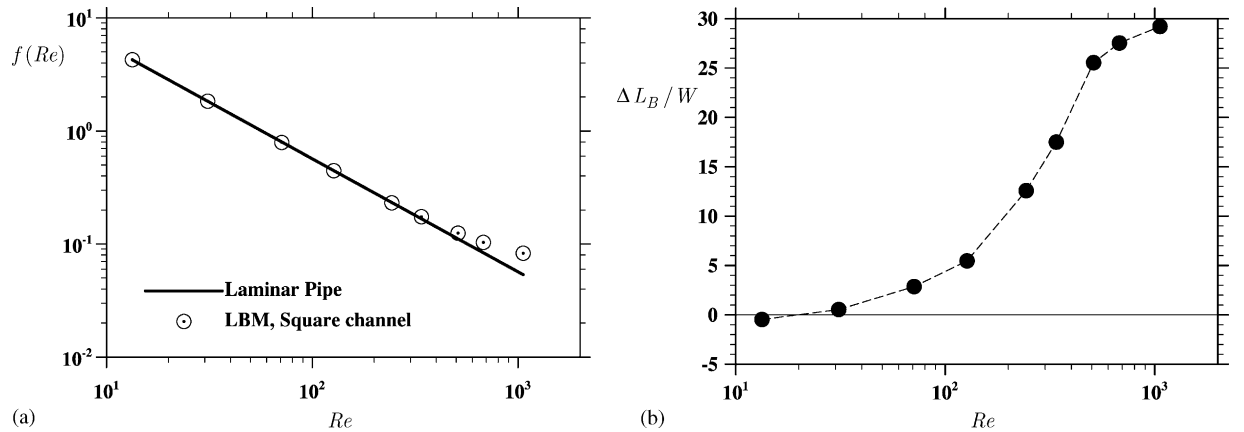

Fig. 4. (a) The friction factor for the straight portion of the channel away from the bend. (b) The augmented loss due to the bend measured as the equivalent length of a straight channel.

actual single-path length in a typical PEMFC, implying that the bend pressure loss must be considered in fuel-cell flow modeling. The slight negative value at the lowest *Re* is due to the fact that the flow can make 180-degree turn along the inner bend at such low *Re*. We note that the curve in Fig. 4(b) is very similar to Fig. 9(b) in Maharudrayya et al. [7], both showing a rapid increase of the bend loss with *Re* for *Re* on the order of 100, although the geometric parameter of the bend was not matched exactly.

Finally, a complex flow pattern is observed at $Re \approx 1000$ (Fig. 5). It appears that the flow in the bend region becomes unstable and small-scale vortices form, as seen in both *x*–*y* and the *z*–*y* planar views in Fig. 5. To our knowledge, no accurate simulations for this *Re* range for a serpentine channel were made previously. Further analysis of this *Re* dependence will be reported in detail in a separate paper.

3. Flow through a channel filled or partially filled with porous medium

This section is motivated by the need to consider the interface between porous medium and clear flow channel in PEMFC modeling. We first consider flow in a 2D channel filled with porous medium of given porosity ϵ and permeability *K*. The macroscopic variables averaged over a representative elementary volume (REV) [2,8] are considered and they

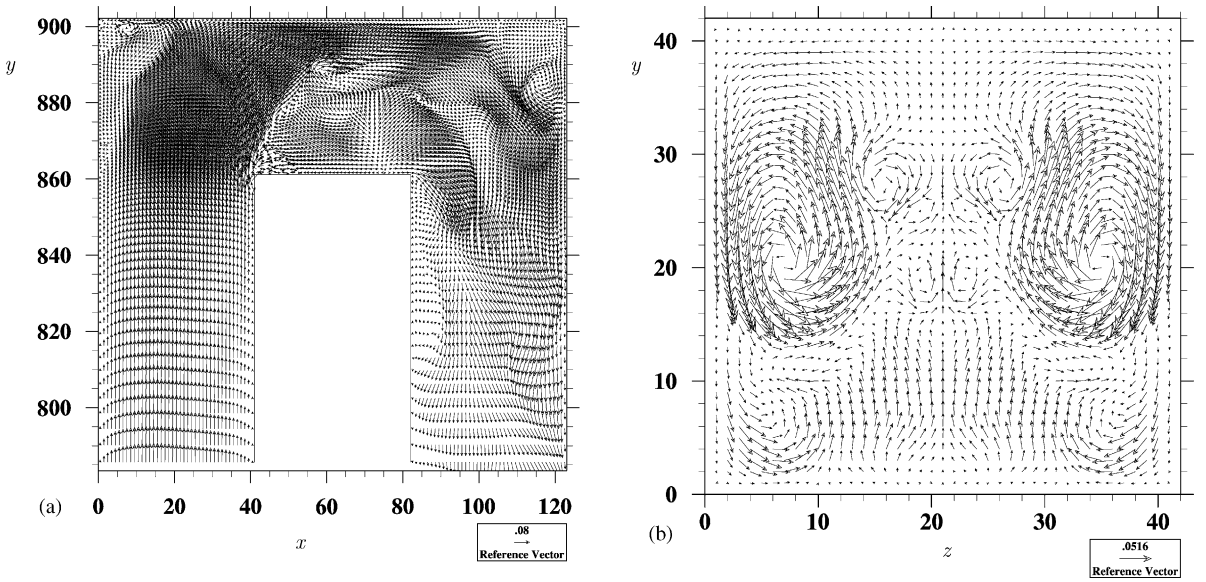

Fig. 5. A snapshot of the quasi-steady velocity field in (a) the x–y plane through the middle of the channel and (b) the z–y plane through the middle of the bend, for $Re = 1059$.

are governed by the following momentum equation incorporating a Brinkman-extended Darcy law:

$$\frac{\partial \mathbf{u}}{\partial t} + (\mathbf{u}\cdot\nabla)\left(\frac{\mathbf{u}}{\epsilon}\right) = -\frac{1}{\rho}\nabla(\epsilon p) + \nu_e\nabla^2\mathbf{u} + \mathbf{F} \quad \text{with } \mathbf{F} = -\frac{\epsilon\nu}{K}\mathbf{u} - \frac{\epsilon F_\epsilon}{\sqrt{K}}|\mathbf{u}|\mathbf{u} + \epsilon\mathbf{G}, \tag{5}$$

where the REV-averaged velocity $\mathbf{u}$ is assumed to be divergence-free, ν is fluid viscosity, ν_e is an effective viscosity, G represents the driving force for the flow. The geometric factor F_ϵ depends on the porosity and the microscopic configuration of porous medium (for details, see Refs. [2,8]). This approach recovers the usual Navier–Stokes equation if $\epsilon \to 1$.

An LB model for the above macroscopic partial differential equation has been rigorously derived by Guo and Zhao [2]. The LB equation is identical to Eq. (1), but with f_i^{eq} and ψ_i modified as

$$f_i^{(\mathrm{eq})} = \omega_i\rho\left[1 + \frac{\mathbf{e}_i\cdot\mathbf{u}}{c_s^2} + \frac{\mathbf{uu}:(\mathbf{e}_i\mathbf{e}_i - c_s^2\mathbf{I})}{2\epsilon c_s^4}\right], \qquad \psi_i = \omega_i\left(1 - \frac{1}{2\tau}\right)\left[\frac{\mathbf{e}_i\cdot\mathbf{F}}{c_s^2} + \frac{\mathbf{uF}:(\mathbf{e}_i\mathbf{e}_i - c_s^2\mathbf{I})}{\epsilon c_s^4}\right]. \tag{6}$$

We first apply the above model to a 2D channel of width H filled with porous medium. The flow is initially at rest and is driven by a constant pressure gradient G along the flow direction. In this case, the unidirectional transient flow subjected to the boundary conditions $u(y=0,t) = u(y=H,t) = 0$ can be solved analytically, giving:

$$u(y,t) = \frac{GK}{\nu}\left\{1 - \frac{\cosh[r(y-0.5H)]}{\cosh[0.5rH]}\right\} - \sum_{k=1,3,5,\ldots}^{\infty}\frac{4GK}{\nu}\frac{(\pi k)^2}{(\pi k)^2 + (rH)^2}\sin\frac{\pi k y}{H}$$
$$\times \exp\left\{-[(\pi k)^2 + (rH)^2]\frac{\nu_e t}{H^2}\right\}, \tag{7}$$

where $r \equiv \sqrt{\nu\epsilon/(\nu_e K)}$. The analytical solution implies that there are two time scales in this problem, a diffusion time scale across the channel $T_1 \equiv H^2/(\pi^2\nu_e)$ and a diffusion time scale within the porous medium $T_2 \equiv K/(\epsilon\nu)$. The ratio of the two time scales T_2/T_1 is equal to $\pi^2 Da/\epsilon$, which can be very small if the permeability is small. Here the Darcy number is defined as K/H^2. We find that in the implementation of the above LB scheme, it may be necessary to use a very small Darcy velocity or a large H to ensure that both T_1 and T_2 are much larger than one. Otherwise, an apparent slip may be present near the walls (Fig. 6a), regardless whether the midway bounce-back or the nonequilibrium extrapolation method [4] was used on the walls. The value of Δt is the time interval between the different curves in the lattice unit. This slip disappears and the analytical solution can be precisely recovered when $T_1 \gg 1$ and $T_2 \gg 1$. A permissible lower bound for the time scales is found to be about 50 lattice time units.

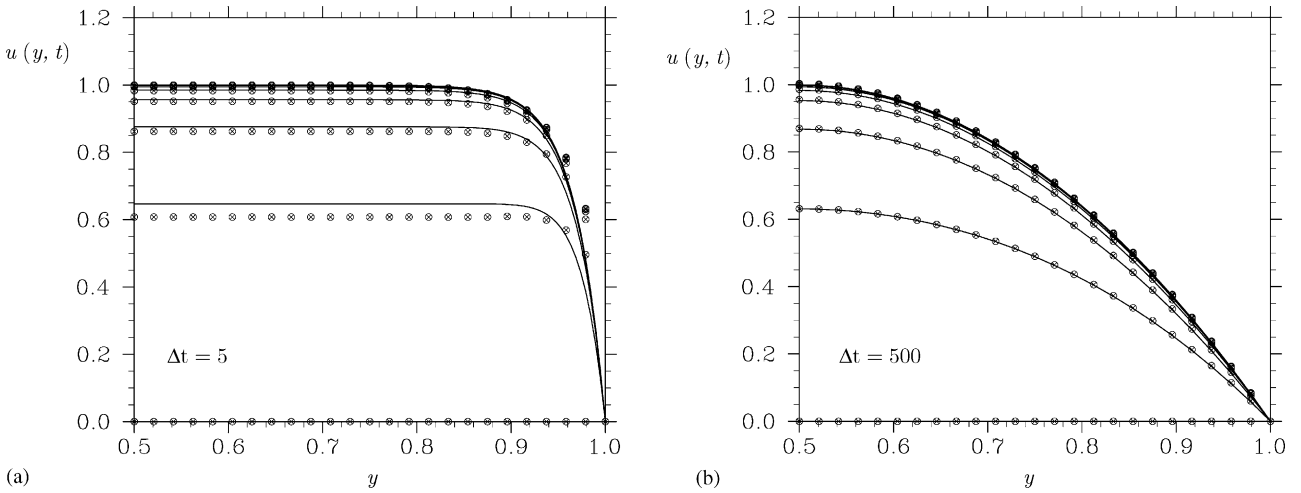

Fig. 6. Comparison of velocity profiles from LB model (symbols) with the analytical solution (lines) at different times. Only a half of the channel is plotted due to the symmetry. The centerline velocity was set to 0.001, $Re = 0.1$, and $H = 48$, yielding $T_1 \approx 487$. (a) Porous medium with $Da = 0.0001$ and $\epsilon = 0.1$, which resulted in $T_2 = 4.8$ only; (b) $Da = 10000$ and $\epsilon = 0.9999$, which approaches the clear channel.

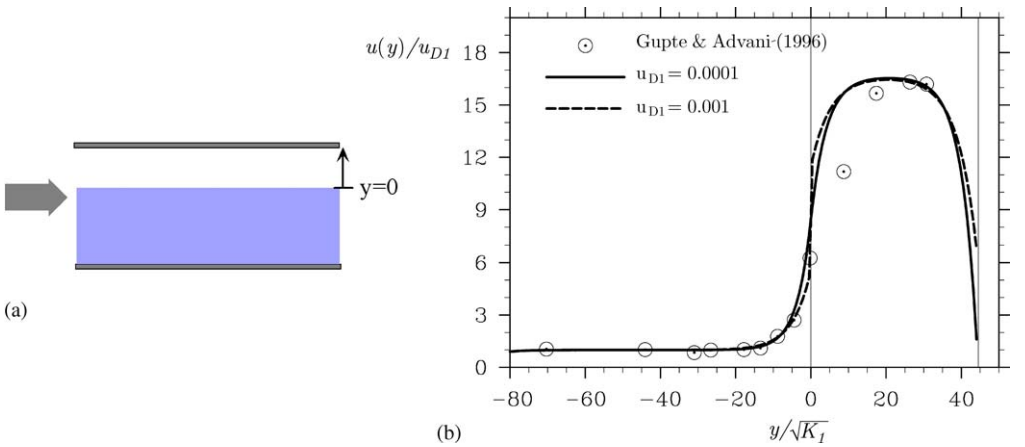

Fig. 7. Velocity profile in a 2D channel partially filled with porous medium (see the sketch of the domain on the left). Parameters are: $\epsilon = 0.07$, $Re = 0.107$, $K_c/K_1 = 16.634$, and $Da = 5.611\text{E}{-5}$. Only a part of the channel is shown. The interface is located at $y = 0$.

Finally, we simulated flow in a channel partially filled with porous medium so there is an interface inside the channel (Fig. 7). The velocity varies continuously across the interface only when a very small Dracy velocity u_{D1} in the porous medium region was used (Fig. 7), for the reason indicated above. Two different treatments near the interface were tested. The first method places the interface in between the lattice nodes so that only the streaming step lead to exchanges of DF between two sides of the interface. The second method treats the interface as a boundary using the nonequilibrium extrapolation method, with the density and velocity taken as the average value from the two neighboring lattice points on the two sides of the interface. The results from the two treatments are almost identical. The results are also compared in Fig. 7 with the experimental data of Gupte and Advani [5]. The discrepancy in the clear channel region near the interface may be caused by the fact that the interface is not sharply defined in the experiment. Further investigation is underway to understand the origin of this discrepancy.

4. Conclusions

Two flow problems relevant to PEMFC are simulated with the LB approach. A 3D viscous flow through a section of serpentine channel has been simulated and is shown to depend sensitively on the flow Reynolds number as the flow Reynolds number is increased from 10 to 1000. The pressure distribution along both the straight portion and bend

region of the channel can be quantitatively modeled. There also appears to be some evidence that the transition to a turbulent flow occurs at Reynolds number on the order of 1000. We also demonstrate that flow through a porous medium with an interface can be treated with the LB approach, provided that the existence of multiple macroscopic time scales is taken into consideration. Our next step would be to integrate the two problems to study fluid flow in PEMFC with both the clear channel and the gas diffusion layer [12].

Acknowledgements

This study is supported by the U.S. Department of Energy. The authors thank Professor Suresh Advani and Professor Ajay Prasad of University of Delaware for helpful discussions.

References

[1] S. Chen, G. Doolen, Annu. Rev. Fluid Mech. 30 (1998) 329–364.
[2] Z. Guo, T.S. Zhao, Phys. Rev. E 66 (2002) 036304.
[3] Z. Guo, C. Zheng, B. Shi, Phys. Rev. E 65 (2002) 046308.
[4] Z. Guo, C. Zheng, B. Shi, Chin. Phys. 11 (2002) 366–374.
[5] S.K. Gupte, S.G. Advani, Exp. Fluids 22 (1997) 408–422.
[6] X. He, L.-S. Luo, M. Dembo, J. Comp. Phys. 129 (1996) 357–363.
[7] S. Maharudrayya, S. Jayanti, A.D. Deshpande, J. Power Sources 138 (2004) 1–13.
[8] P. Nithiarasu, K.N. Seetharamu, T. Sundararajan, Int. J. Heat Mass Transfer 40 (1997) 3955–3967.
[9] Y. Qian, S. Succi, S.A. Orszag, Annu. Rev. Comput. Phys. 3 (1995) 195–242.
[10] C. Shu, X.D. Niu, Y.T. Chew, Int. J. Mod. Phys. C. 14 (2003) 925–944.
[11] C.Y. Wang, Fundamental models for fuel cell engineering, Chem. Rev. 104 (2004) 4727–4766.
[12] L.P. Wang, B. Afsharpoya, Advances in Fluid Mechanics, in: M. Rahman, C.A. Brebbia (Eds.), vol. VI, WIT press, Southampton, UK, 2006, pp. 287–296.